Fully-Connected-Based Adaptive Speckles Optimization Method for Ghost Imaging

Yu Zhou, Shuai Mao, Yuchen He, *Member, IEEE*, Juan Chen, Hui Chen, Huaibin Zheng, Jianbin Liu, and Zhuo Xu

***Abstract*— Ghost imaging (GI) has recently emerged as a promising new imaging technology, generating considerable interest in the field. Using appropriate speckles in GI can result in higher-quality reconstructed target images. The conventional method of projecting random speckles to illuminate unknown targets often results in low efficiency and poor image reconstruction quality. Recently, we find that speckles in GI act similarly to fully-connected layers in neural networks, in terms of information processing and transmission. Therefore, we propose an improved projection method for speckles, called AGOS, which is based on adaptive gradient optimization employing a fully-connected layer. Demonstrations based on simulations and experiments show that the proposed method in this letter can achieve better results than random speckles under the same conditions.**

***Index Terms*— Ghost imaging, speckles optimization, deep learning, fully-connected layer.**

I. Introduction

GHOST imaging (GI), as a relatively new imaging technology, was first completed experimentally by Pittman and Shih in 1995 [1]. Since then, various researchers have explored the potential of GI and have made notable contributions to its development [2], [3], [4], [5], [6], [7]. In 2008, computational ghost imaging (CGI) was proposed by Shapiro [8], in which the wavefront information when reaching an object can be obtained by calculation. However, obtaining high-quality results at low sampling rates using random projection in GI remains a challenge. While various methods such as differential ghost imaging (DGI) [9] and normalized ghost imaging (NGI) [10] have been proposed based on basic correlation (BC) to enhance the quality of reconstructed images, these methods still require a large number of measurements over a long period of time. In 2009, the compressed sensing (CS) algorithm was brought to GI [11]. Due to the strong vitality of deep learning in the field of optical metrology [12], deep learning methods have been introduced to GI since 2017 [13], [14], [15], [16], [17], [18]. Besides, studies on Hadamard matrices [19], [20], [21], discrete cosine transfer [22] and principal component analysis [23] have also been carried out to reduce the sampling rate of GI. For the previous methods, conventional speckles were utilized without taking target features into consideration. Inspired by a study in CS [24], a speckle optimizing method based on adaptive gradient optimization called AGOS was proposed in this letter, which can generate adaptive speckles with the help of gradient information. AGOS GI system is shown in Fig.1.

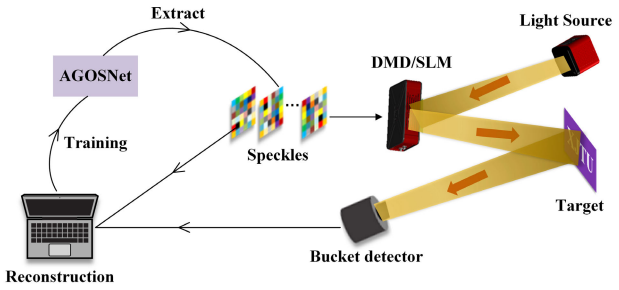

Fig. 1. AGOS ghost imaging system.

In this work, speckles are regarded as fully-connected layer parameters that can be extracted from the first layer of AGOSNet neural network. These adaptive speckles are then projected onto targets using Digital Micromirror Device (DMD) or Spatial Light Modulator (SLM). During the training phase, speckles are optimized adaptively in the process of gradient descent. To demonstrate the efficacy of the proposed method, the AGOSNet is firstly employed at 1% and 5% sampling rates to reconstruct targets, and the results are compared with those of random speckles. Subsequently, the adaptive speckles are extracted from the aforementioned AGOSNet and used in conjunction with a CS algorithm called fast iterative shrinkage-thresholding algorithm (FISTA) [25] to reconstruct targets, and the results are once again compared with those of

Manuscript received 20 June 2023; revised 16 July 2023; accepted 26 July 2023. Date of publication 31 July 2023; date of current version 9 August 2023. This work was supported in part by the National Natural Science Foundation of China under Grant 61901353, in part by the Fundamental Research Funds for the Central Universities under Grant xhj032021005, in part by the Key Research and Development Projects of Shaanxi Province under Grant 2021GXLH-Z-012, in part by the 111 Project of China under Grant B14040, and in part by the Project of JD AI Research under Grant 202105127. *(Corresponding author: Yuchen He.)*

Yu Zhou is with the MOE Key Laboratory for Nonequilibrium Synthesis and Modulation of Condensed Matter, Department of Applied Physics, Xi'an Jiaotong University, Xi'an 710049, China (e-mail: zhou1@xjtu.edu.cn).

Shuai Mao and Juan Chen are with the School of Information and Communications Engineering, Xi'an Jiaotong University, Xi'an 710049, China (e-mail: a67140915@stu.xjtu.edu.cn; chen.juan.0201@mail.xjtu.edu.cn).

Yuchen He, Hui Chen, Huaibin Zheng, Jianbin Liu, and Zhuo Xu are with the Electronic Materials Research Laboratory, Key Laboratory of the Ministry of Education and International Center for Dielectric Research, School of Electronic Science and Engineering, Xi'an Jiaotong University, Xi'an 710049, China (e-mail: yuchenhe@xjtu.edu.cn; chenhui@xjtu.edu.cn; huaibinzheng@xjtu.edu.cn; liujianbin@xjtu.edu.cn; xuzhuo@xjtu.edu.cn).

Color versions of one or more figures in this letter are available at https://doi.org/10.1109/LPT.2023.3300092.

Digital Object Identifier 10.1109/LPT.2023.3300092

1041-1135 © 2023 IEEE. Personal use is permitted, but republication/redistribution requires IEEE permission.
See https://www.ieee.org/publications/rights/index.html for more information.

Authorized licensed use limited to: Xian Jiaotong University. Downloaded on September 05,2023 at 13:24:41 UTC from IEEE Xplore. Restrictions apply.

random speckles. Finally, we design an experimental demonstration of the proposed method. It can be proven that with our adaptive speckles, GI can reconstruct images with higher quality.

II. Method

Our idea comes from the CGI framework. A typical CGI process can be described by the following equations:

$$Sr_i = \int\int S_i(x, y) \times O(x, y) dxdy, \tag{1}$$

where S_i is the i^{th} illumination speckle, Sr_i is the i^{th} transmitted or reflected signal received by a bucket detector, $O(x, y)$ is the feature function that characterizes target object.

$$Image(x, y) = f^{Recon}(Sr_{i:N}, S_{i:N}), \tag{2}$$

where f^{Recon} stands for the complex process of image reconstruction. Since the bucket signal is strongly dependent on speckles and objects, we can transform Eq.2 to Eq.3.

$$Image(x, y) = f^{Recon}(S_{i:N}, O(x, y)). \tag{3}$$

A direct idea from Eq.3 is to get the gradient information, with which we can make the reconstructed image as close to the object as possible. However, GI algorithms are usually accompanied by iterations, which makes them hard to obtain the gradient information.

Here, we turn to neural networks (NN) for help, which have two advantages. The first is that NN have a strong approximation ability as it can use linear functions to approximate nonlinear functions. The second is that the gradient information can be easily obtained. Further, the bucket detector used in GI is without spatial resolution, which is shown in Eq.1 – the bucket signals received by a bucket detector are an integration, in other words, 2D summation of the interaction result between speckles and the feature function of the target. This process can be modeled by a fully-connected layer in NN. As shown in the bottom of Fig. 2, if biases are not used in a fully-connected layer, then the outputs are equivalent to the input multiplied by the weights and then added together. Thus, speckles can be seen as the weights of a fully-connected layer. Since each output corresponds to one measurement process, the sampling rate can be controlled by adjusting the number of outputs. This also allows the AGOSNet to reconstruct images at different sampling rates. From this point, we propose an AGOSNet shown in Fig.2.

The AGOSNet is designed to optimize the measurement and image reconstruction simultaneously. The first layer in AGOSNet is a fully-connected layer that generates adaptive speckles. The subsequent layers, called ReconNet [26], are responsible for image reconstruction given the inputs. In AGOSNet, an input image is first reshaped into a column vector and passed through the fully-connected layer, which represents the measurement process and generates bucket signals. The bucket signals are then up-sampled using another fully-connected layer to match the original image size. Six convolutional layers are used to extract image features and reconstruct the target image. The network structure and corresponding inputs and outputs are shown in Fig.2. Once the AGOSNet is well-trained, adaptive speckles can be obtained by extracting the parameters from the first fully-connected layer. The corresponding bucket signals can then be used as inputs at the second fully-connected layer to reconstruct the target image.

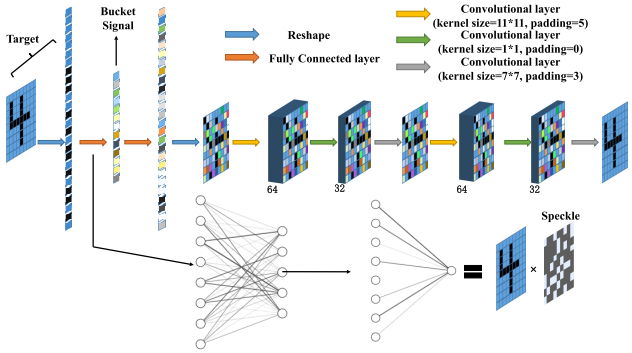

Fig. 2. AGOSNet structure.

III. Demonstrations Results Based on Simulations

In this first stage, our method is validated by assessing its performance through simulation results. To obtain adaptive speckles, 100 intact complex images in the size of 481*313 or 313*481 from the BSDS dataset [27] are used to train AGOSNet. Each image is divided into blocks in size of 33*33 with a stride of 14, which leads to 64000 image blocks. Each image block will be reshaped into a column vector as input. The initial image blocks are set as labels. We use the Adam optimizer to optimize the mean square error loss function between network outputs and labels.

A. AGOSNet Demonstration Based on Complex Targets

Firstly, AGOSNet is used to evaluate our adaptive speckles. More specifically, complex target images are illuminated using adaptive speckles and random speckles at 1% and 5% sampling rates, respectively. The resulting bucket signals are then passed through AGOSNet to obtain reconstruction results. The quality of the reconstructed images was measured using the peak signal-to-noise ratio (PSNR) and the structure similarity index measure (SSIM). The reconstruction results are shown in Fig.3. An overview of the PNSR and SSIM results is provided in Table.I. It shows that our adaptive speckles are more efficient than random speckles. The PSNR results increase by around 9 dB and SSIM results rise by around 0.3 at the sampling rate of 1% and 5%, which is a huge improvement that is hard to achieve using other methods.

B. AGOS Demonstration Based on CS Algorithm

In addition to using AGOSNet for reconstruction, we also compared the performance of AGOS adaptive speckles and random speckles in conjunction with the FISTA algorithm. The same targets and sampling rates as in the previous subsection were used. The reconstruction results in terms of PSNR and SSIM are shown in Fig.4. Although the results were not obtained through the network, the imaging quality

Authorized licensed use limited to: Xian Jiaotong University. Downloaded on September 05,2023 at 13:24:41 UTC from IEEE Xplore. Restrictions apply.

TABLE I
RECONSTRUCTION RESULTS OF AGOSNET AT DIFFERENT SAMPLING RATES

Sampling Rate	Speckles	boat		bird		house		path		starfish		statue		tiger	
		psnr	ssim	psnr	ssim	psnr	ssim	psnr	ssim	psnr	ssim	psnr	ssim	psnr	ssim
1%	adaptive	18.0057	0.5327	18.1833	0.5839	21.2558	0.3956	24.0649	0.5023	19.9457	0.4339	22.5953	0.5316	19.4202	0.1972
	random	9.6852	0.1398	10.7674	0.1334	12.6221	0.1304	13.9955	0.161	12.8263	0.1654	12.6995	0.1369	14.0968	0.0903
	increment	**8.3205**	**0.3929**	**7.4159**	**0.4505**	**8.6337**	**0.2652**	**10.0694**	**0.3413**	**7.1194**	**0.2685**	**9.8958**	**0.3947**	**5.3234**	**0.1069**
5%	adaptive	21.9331	0.6186	21.13	0.6483	22.4369	0.4494	25.9988	0.5884	22.453	0.5731	24.6861	0.6149	20.0844	0.2457
	random	10.4479	0.1378	11.2474	0.1173	12.5734	0.1548	13.9879	0.1782	12.5878	0.171	12.6118	0.1739	14.3331	0.109
	increment	**11.4852**	**0.4808**	**9.8826**	**0.531**	**9.8635**	**0.2946**	**12.0109**	**0.4102**	**9.8652**	**0.4021**	**12.0743**	**0.441**	**5.7513**	**0.1367**

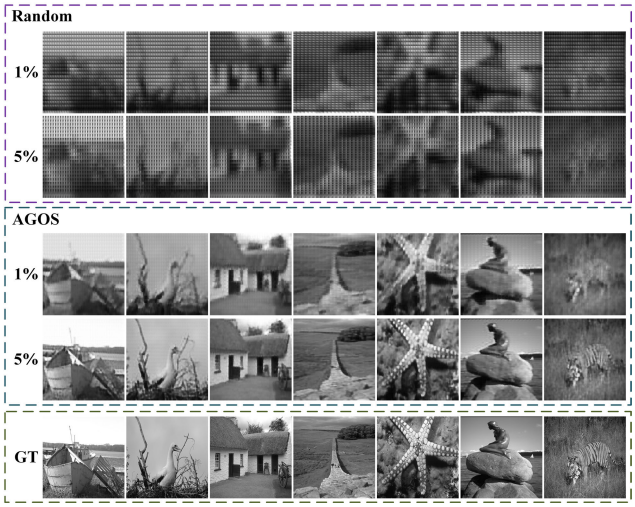

Fig. 3. Reconstruction results of AGOSNet at different sampling rates.

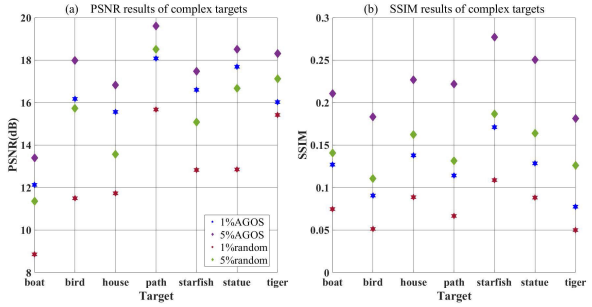

Fig. 4. Complex targets results of FISTA at different sampling rates.

of adaptive speckles is better than that of random speckles at both sampling rates. Even at a low sampling rate of 1%, the results obtained with adaptive speckles are better than those obtained with random speckles, with a 5 dB improvement for targets such as the bird and the statue.

C. Demonstration Based on Dynamic Targets

Furthermore, targets may be moving in actual scenes. So simulations are organized to verify the effectiveness of AGOS on dynamic targets. We used the target "XJTU" and applied different translation pixels and rotation angles to it. The reconstruction results of the translated and rotated targets at a sampling rate of 25% are presented in Fig.5.

The corresponding average PSNR and SSIM results are shown on the right side of Fig.5. It is evident that the adaptive speckles are also efficient in dynamic scenarios, as the PSNR approximately doubled on average and the SSIM also

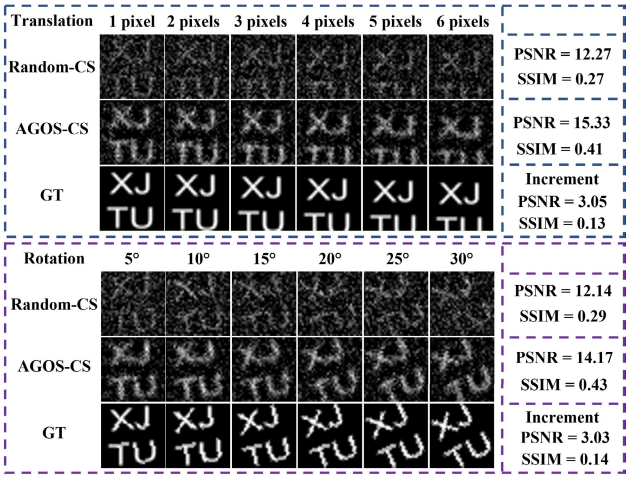

Fig. 5. Dynamic results under SR of 25%.

increased by an average of 0.14. These results demonstrate the effectiveness of the AGOS method in dynamic scenarios.

D. Speckle Property Analysis

Correlation coefficient matrixes of our adaptive speckles and random speckles are calculated to analyze the speckle property. According to our calculation, our adaptive speckles have larger correlation coefficients. To explain this, it is worth noticing that not all information in different image areas is equally important. The area containing more information called the active area should be deserved more attention. The values in the active area will be larger to highlight information. As a result, they will be more correlated. When the signals are collected by the bucket detector, more important information will be obtained to reconstruct the target image. This is the reason why our speckles can achieve better results.

IV. DEMONSTRATIONS BASED ON PHYSICAL EXPERIMENTS

In real-world scenarios, the effectiveness of our method can be influenced by environmental disturbances and mutual interference among light sources. To address this, physical experiments were conducted to showcase the efficacy of our proposed method. The experiment schematic diagram is shown in Fig.6. A letter "N" was used as the target. Speckles, sized at a resolution of 32×32, are extracted from the first fully-connected layer of an AGOSNet at a sampling rate of 25%. These speckles are subsequently loaded onto a DMD, which is used to modulate the light emitted from the light source. The light source and DMD are integrated within the

Authorized licensed use limited to: Xian Jiaotong University. Downloaded on September 05,2023 at 13:24:41 UTC from IEEE Xplore. Restrictions apply.

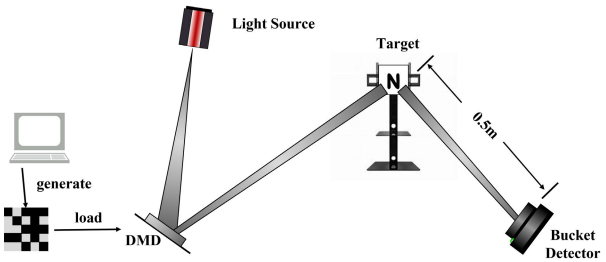

Fig. 6. Experimental schematic diagram.

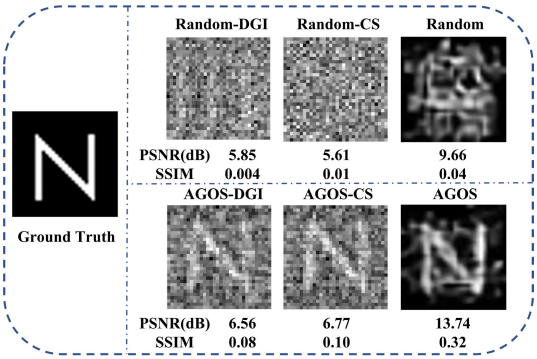

Fig. 7. Physical experimental results at SR = 25% using DGI, FISTA, and AGOSNet.

WeiMai-M200. Subsequently, the modulated light was directed toward the target, illuminating it accordingly. Following the propagation of light through a distance of half a meter, the corresponding reflected signals were collected by a Thorlabs DET025A/M bucket detector.

To verify that our adaptive speckles are better than random speckles, three different algorithms were used to reconstruct targets using bucket signals and corresponding speckles. Among the three algorithms mentioned, DGI refers to the traditional GI algorithm, FISTA stands for the GI algorithm based on CS, and AGOS represents the GI algorithm based on deep learning. The final reconstruction results are shown in Fig. 7. The reconstructed results in the second row are obtained by employing adaptive speckles, whereas the results in the first row are obtained using random speckles. It can be clearly found that when using our adaptive speckles, the target can be reconstructed, but when using random speckles, the target is submerged in noise. This finding significantly demonstrates the effectiveness of our adaptive speckles in real scenes.

V. Conclusion

In this letter, we have demonstrated that speckles in GI exhibit similarities to fully-connected layers in NN. Based on the fully-connected layer, our proposed approach enables better utilization of gradient information. It is evident that using our adaptive speckles leads to improved image reconstruction quality. For complex images, an average increase of approximately 9 dB for PSNR and a rise of about 0.3 for SSIM results can be achieved at the sampling rate of 1% and 5%, respectively, using the AGOSNet system. For dynamic images, our AGOS-based approach resulted in an average increase of about 3 dB for PSNR. Results of physical experiments further validate the effectiveness of our method in real scenarios.

References

[1] T. B. Pittman, Y. H. Shih, D. V. Strekalov, and A. V. Sergienko, "Optical imaging by means of two-photon quantum entanglement," *Phys. Rev. A, Gen. Phys.*, vol. 52, no. 5, pp. R3429–R3432, Nov. 1995.

[2] R. S. Bennink, S. J. Bentley, and R. W. Boyd, "'Two-photon' coincidence imaging with a classical source," *Phys. Rev. Lett.*, vol. 89, no. 11, 2002, Art. no. 113601.

[3] R. Meyers, K. S. Deacon, and Y. Shih, "Ghost-imaging experiment by measuring reflected photons," *Phys. Rev. A, Gen. Phys.*, vol. 77, no. 4, p. 41801, Apr. 2008.

[4] Y. Bromberg, O. Katz, and Y. Silberberg, "Ghost imaging with a single detector," *Phys. Rev. A, Gen. Phys.*, vol. 79, no. 5, p. 53840, May 2009.

[5] Y. Wang, J. Suo, J. Fan, and Q. Dai, "Hyperspectral computational ghost imaging via temporal multiplexing," *IEEE Photon. Technol. Lett.*, vol. 28, no. 3, pp. 288–291, Feb. 1, 2016.

[6] Z. Pan and L. Zhang, "Optical cryptography-based temporal ghost imaging with chaotic laser," *IEEE Photon. Technol. Lett.*, vol. 29, no. 16, pp. 1289–1292, Aug. 15, 2017.

[7] J. Tang, D. Zou, M. Cheng, L. Deng, D. Liu, and M. Zhang, "Single-shot temporal ghost imaging based on orthogonal frequency-division multiplexing," *IEEE Photon. Technol. Lett.*, vol. 30, no. 17, pp. 1555–1558, Sep. 1, 2018.

[8] J. H. Shapiro, "Computational ghost imaging," *Phys. Rev. A, Gen. Phys.*, vol. 78, no. 6, p. 61802, Dec. 2008.

[9] F. Ferri, D. Magatti, L. A. Lugiato, and A. Gatti, "Differential ghost imaging," *Phys. Rev. Lett.*, vol. 104, no. 25, Jun. 2010, Art. no. 253603.

[10] B. Sun, S. S. Welsh, M. P. Edgar, J. H. Shapiro, and M. J. Padgett, "Normalized ghost imaging," *Opt. Exp.*, vol. 20, no. 15, pp. 16892–16901, 2012.

[11] O. Katz, Y. Bromberg, and Y. Silberberg, "Compressive ghost imaging," *Appl. Phys. Lett.*, vol. 95, no. 13, Sep. 2009, Art. no. 131110.

[12] C. Zuo et al., "Deep learning in optical metrology: A review," *Light, Sci. Appl.*, vol. 11, no. 1, p. 39, Feb. 2022.

[13] M. Lyu et al., "Deep-learning-based ghost imaging," *Sci. Rep.*, vol. 7, no. 1, pp. 1–6, Dec. 2017.

[14] Y. He et al., "Ghost imaging based on deep learning," *Sci. Rep.*, vol. 8, no. 1, pp. 1–7, Apr. 2018.

[15] H. Wu et al., "Deep-learning denoising computational ghost imaging," *Opt. Lasers Eng.*, vol. 134, Nov. 2020, Art. no. 106183.

[16] H. Wu et al., "Sub-Nyquist computational ghost imaging with deep learning," *Opt. Exp.*, vol. 28, no. 3, pp. 3846–3853, 2020.

[17] Y. He, S. Duan, Y. Yuan, H. Chen, J. Li, and Z. Xu, "Semantic ghost imaging based on recurrent-neural-network," *Opt. Exp.*, vol. 30, no. 13, pp. 23475–23484, 2022.

[18] F. Wang et al., "Far-field super-resolution ghost imaging with a deep neural network constraint," *Light, Sci. Appl.*, vol. 11, no. 1, p. 1, 2022.

[19] L. Wang and S. Zhao, "Fast reconstructed and high-quality ghost imaging with fast Walsh–Hadamard transform," *Photon. Res.*, vol. 4, no. 6, pp. 240–244, 2016.

[20] M.-J. Sun, L.-T. Meng, M. P. Edgar, M. J. Padgett, and N. Radwell, "A Russian dolls ordering of the Hadamard basis for compressive single-pixel imaging," *Sci. Rep.*, vol. 7, no. 1, p. 3464, Jun. 2017.

[21] W.-K. Yu, "Super sub-Nyquist single-pixel imaging by means of cake-cutting Hadamard basis sort," *Sensors*, vol. 19, no. 19, p. 4122, Sep. 2019.

[22] B.-L. Liu, Z.-H. Yang, X. Liu, and L.-A. Wu, "Coloured computational imaging with single-pixel detectors based on a 2D discrete cosine transform," *J. Mod. Opt.*, vol. 64, no. 3, pp. 259–264, Feb. 2017.

[23] G. Wang et al., "De-noising ghost imaging via principal components analysis and compandor," *Opt. Lasers Eng.*, vol. 110, pp. 236–243, Nov. 2018.

[24] X. Xie, Y. Wang, G. Shi, C. Wang, J. Du, and X. Han, "Adaptive measurement network for CS image reconstruction," in *Proc. CCF Chin. Conf. Comput. Vis.* Singapore: Springer, 2017, pp. 407–417.

[25] A. Beck and M. Teboulle, "A fast iterative shrinkage-thresholding algorithm for linear inverse problems," *SIAM J. Imag. Sci.*, vol. 2, no. 1, pp. 183–202, Jan. 2009.

[26] K. Kulkarni, S. Lohit, P. Turaga, R. Kerviche, and A. Ashok, "ReconNet: Non-iterative reconstruction of images from compressively sensed measurements," in *Proc. IEEE Conf. Comput. Vis. Pattern Recognit. (CVPR)*, Jun. 2016, pp. 449–458.

[27] D. Martin, C. Fowlkes, D. Tal, and J. Malik, "A database of human segmented natural images and its application to evaluating segmentation algorithms and measuring ecological statistics," in *Proc. 8th IEEE Int. Conf. Comput. Vis. (ICCV)*, vol. 2, Jul. 2001, pp. 416–423.

Authorized licensed use limited to: Xian Jiaotong University. Downloaded on September 05,2023 at 13:24:41 UTC from IEEE Xplore. Restrictions apply.